Analysis of Moving-Coil Actuator Jet Injectors for Viscous Fluids

Rhys M. J. Williams*, Bryan P. Ruddy, *Member, IEEE*, N. Catherine Hogan, Ian W. Hunter, Poul M. F. Nielsen, *Member, IEEE* and Andrew J. Taberner, *Member, IEEE*

***Abstract*— *Objective:* A jet injector is a device that can be used to deliver liquid drugs through the skin using a fluid jet, without the use of a needle. Most jet injectors are designed and used for the delivery of inviscid liquids, and are not optimized for the delivery of viscous drug compounds. To better understand the requirements for delivering viscous drugs, we have developed a mathematical model of the electro-mechanics of a moving-coil actuated jet injector as it delivers viscous fluids. *Methods:* The model builds upon previous work by incorporating the non-linear electrical properties of the motor, compliant elements of the mechanical piston and ampoule system, and the effect of viscosity on injector characteristics. The model has been validated by monitoring the movement of the piston tip and measurements of the jet force. *Results:* The results of the model indicate that jet speed is diminished with increasing fluid viscosity, but overshoot and ringing in the jet speed is unaffected. However, a stiffer ampoule and piston will allow for better control of the jet speed profile during an injection, and reduce ringing. *Conclusion:* We identified that the piston friction coefficient, the compliance of the injector components, and the viscous properties of the fluid are important determinants of performance when jet injecting viscous fluids. *Significance:* By expanding upon previous jet injector models, this work has provided informative simulations of jet injector characteristics and performance. The model can be used to guide the design of future jet injectors for viscous fluids.**

***Index Terms*— Drug delivery, Biomedical electronics, Actuators, Fluid flow control, Viscosity**

I. INTRODUCTION

DRUGS designed to be absorbed in the tissue underneath the skin are typically delivered by needle and syringe. This method causes pain and is prone to needle-stick injuries for medical professionals [1]. A jet injector (JI) is a device that forms a fluid jet that can pierce through the skin and deliver drugs to dermal, subcutaneous, and muscular tissue in humans and animals [2]. The delivery is achieved without the risk of needle-stick injuries and with reduced or equivalent levels of pain compared to the needle and syringe method [3]–[5]. In these systems, force is applied to a piston that increases the pressure within a fluid-filled ampoule; the pressure forces the fluid to form a jet that ejects from a small orifice at the opposite end of the ampoule. The force can be applied by a variety of different means including compressed gas [6], springs [7], [8], piezoelectric actuators [9], and Lorentz-force actuators [10].

Current JI technology is unable to deliver viscous fluids, such as glycerol, as effectively as low viscosity solutions [11]. Many modern drug formulations, such as monoclonal antibodies, are created in high concentrations and exhibit high viscosity (between 0.01 Pa·s and 0.1 Pa·s) [12]. These formulations are used to treat inflammatory and allergic diseases, cancer, and asthma, and may be more beneficially delivered by controllable jet injection [12], [13]. However, to develop devices for jet-delivery of viscous drugs, we require a more complete understanding of the process of pressurizing the mechanical system that forms a viscous jet that is able to pierce through the skin.

To this end, we report on a detailed mathematical model of a jet injector device that uses a moving-coil actuator (sometimes referred to as a voice-coil or Lorentz-force actuator) as the source of force. Such motors allow a much greater degree of control over the device's behavior than other force generating devices. A control system with the motor allows the production of a wider range of jet profiles compared to those achievable when using a spring or compressed gas device [10].

Previous models [14], [15] of such devices have focused

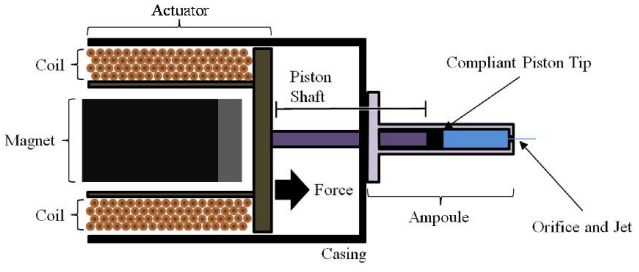

Fig. 1 - Diagram of moving-coil injector system

This paper was submitted on the 21st May 2015 for review. The work described was performed with support from the Vice-Chancellor's Strategic Development fund of the University of Auckland.

*R. M. J. Williams is with the Auckland Bioengineering Institute at the University of Auckland, Auckland, New Zealand (phone: +64 9 373 7599; e-mail: rwil267@aucklanduni.ac.nz).

N. C. Hogan and I. W. Hunter are with the Department of Mechanical Engineering at the Massachusetts Institute of Technology.

B. P. Ruddy, P. M. F. Nielsen and A. J. Taberner are with the Auckland Bioengineering Institute and the Department of Engineering Science at the University of Auckland.

upon the delivery of fluids similar to water in density and viscosity and have not accounted for the influence of viscosity on jet formation. Some (e.g. [14]) have not modeled how voltage applied to a moving-coil motor produces a force that pressurizes the drug, while others (e.g. [15], [16]) have only used first-order models to approximate the response of current and force. Chen et al. [16] model pressure loss due to fluid viscosity using a Darcy friction factor determined from the Moody chart, commonly used for fully-developed flows in constant diameter pipes. However, flows in jet injection are far from fully-developed and pass through large diameter changes. Our model incorporates knowledge about the motor's electrical and mechanical behavior, the impulse response function of current to an applied voltage, and an empirically defined relationship that anticipates pressure losses in the fluid for a given orifice. In addition, we include in our model the non-linear, volume-dependent elastic properties of the piston tip and ampoule.

The model is used to investigate the behavior of a moving-coil actuated jet injector when the mechanical properties of the device and the fluid are modified, and thereby to derive the parameters that are most conducive to jet delivery of viscous fluids.

II. Model Formulation and Parameterization

A. JI System Design

The jet injector (Fig. 1) consists of a moving-coil actuator coupled to a disposable plastic piston (with rubber tip) and ampoule. A 6-layer coil surrounds an NdFeB magnet of 25.4 mm outer diameter. The coil is formed from 0.361 mm (27 AWG) copper wire wound onto a bobbin of 27 mm outer diameter. A potentiometer (ALPS RDC1032) is attached to the coil to measure its position. The piston is made of a polycarbonate shaft with a rubber piston tip that seals the fluid in the ampoule; the total length of the piston is 50 mm. The polycarbonate ampoule has an inner diameter of 3.57 mm and a 190 μm orifice at the far end where the jet emits.

During characterization experiments the actuator's position, voltage, current, and force were measured and/or controlled by a data acquisition and control system (cRIO 9022, National Instruments) with a loop rate of 20 kHz. Tests presented in this text were run in open loop with the voltage generated by the controller at a rate of 20 kHz. All software was written in LabVIEW 2011 (National Instruments). A pair of series-bridged power amplifiers (AE Techron 7224) amplified signals to the coil.

B. Model Formulation

1) Electrical Model: The elements of the injector form a coupled electromechanical and fluidic system that can be described by the block diagram of Fig. 2. In this model, the voltage across the coil (V_C) drives an electrical current in the coil. The current in the coil (I_C) is estimated using the empirically-measured impulse response function of the coil. A finite impulse response filter on the input voltage uses the impulse response function to calculate the current on a point-by-point basis within each simulation time step. The force produced by the coil (F_C) is calculated using K_C as the force constant of the motor (Fig. 2). The force constant is allowed to vary with coil position.

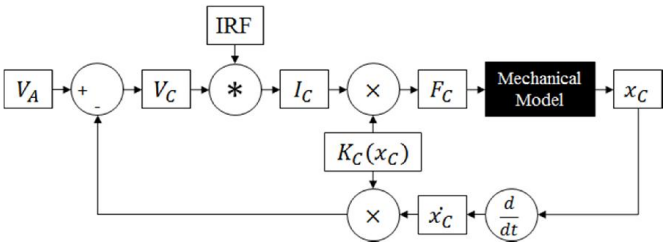

Fig. 2 - Block diagram of JI electromechanical system.

The coil displacement (x_C) is estimated through a nonlinear mechanical model. The velocity of the coil induces a back-EMF in the coil; the back-EMF is the source of a difference between the applied voltage (V_A) and the voltage across the coil.

2) Mechanical Model: The piston has a rubber tip that deforms to seal against the fluid when force is applied to the piston. The model combines the compliance of the tip and the piston shaft by ascribing a non-linear stiffness k_P to the piston (Fig. 3C). The coil's acceleration is described by

$$\ddot{x}_C = \frac{F_C + k_P(x_P - x_C)}{m_C}, \quad (1)$$

where F_C is the force applied by the motor, x_C is the displacement of the coil, x_P is the displacement of the end of the piston tip and m_C is the mass of the coil. The piston tip acceleration is described by

$$\ddot{x}_P = \frac{-k_P(x_P - x_C) - F_{FR} - PA_P}{m_C}, \quad (2)$$

where F_{FR} is the friction force, P is the pressure of the fluid within the ampoule, and A_P is the area of the piston. The mass of the piston is ignored, as it is much less than the coil mass.

Sliding friction arises at the interface between the rubber piston tip and the walls of the ampoule and is proportional to the pressure in the rubber piston tip, which is assumed to be identical to the pressure in the fluid. Therefore, the friction (F_{FR}) is calculated using

$$F_{FR} = \mu A_C P, \quad (3)$$

where A_C is the contact area of the piston tip against the ampoule wall and μ is the friction coefficient [17]. A constant level of static friction is present until the coil starts moving.

At the pressures encountered in jet injection, the compliance of the fluid itself, measured by its bulk modulus, becomes significant. In addition, the ampoule tends to expand under the influence of the high pressure, contributing additional compliance. The ampoule compliance is proportional to the length (and thus the volume) of the fluid column, and can therefore be lumped with the fluid compliance by way of an effective ampoule-fluid bulk modulus (K_{AF}).

A differential equation for the change in pressure over time can be determined via a mass balance [14]. To account for the effective bulk modulus, this equation was slightly modified to

$$\dot{P} = \frac{(K_{AF} + P)\dot{x_P} - \frac{K_{AF}A_O}{A_P}u_O}{x_P}, \quad (4)$$

where A_O is the area of the orifice and u_O is jet speed. The

pressure that results from this equation was applied against the piston as indicated in (2). The pressure loss due to viscous fluid interactions is captured by

$$P_{loss} = \frac{K_D}{2}\rho {u_O}^2, \quad (5)$$

where K_D, the discharge coefficient, is empirically determined and ρ is the density of the fluid. P_{loss} is subtracted from pressure when calculating jet speed. Its formula can be combined with Bernoulli's equation and rearranged to incorporate viscous loss in (4) [17],

$$u_O = \sqrt{\frac{2P}{\rho(1+K_D)}}. \quad (6)$$

The model was implemented in LabVIEW 2011 (National Instruments) using the Runge-Kutta-45 method within the Control and Simulation Module. This solved the model in 0.6 s.

C. Parameter Estimation

1) Coil Impulse Response: A low-noise linear amplifier (KEPCO BOP 50-4D) and the compactRIO previously mentioned were used to evaluate the coil impedance impulse response function. Gaussian white noise of ten volts peak amplitude was applied to the coil. The sample rate of the input and output was 100 kHz. The coil was locked in position at 5 mm from full retraction. The measured voltage and current were used to calculate the impulse response function using stochastic system identification. 500 points of the impulse response function were used. The impulse response function method produced model results that fit measured current values significantly better than a simple first-order series-circuit model of the inductance (4.8 mH) and resistance (9.4 Ω) of the coil (Fig. 3A).

2) Force production over Stroke: A coupling mechanism was manufactured to connect the coil to a load cell. The force was measured at constant current over the stroke of the motor and a 2nd-order polynomial of force constant was fit to the results. The average force constant over the stroke length of the injector (Fig. 3B) was 8.78 $N \cdot A^{-1}$ and exhibited a standard deviation of 1.58 $N \cdot A^{-1}$. The maximum force constant measured was 10.2 $N \cdot A^{-1}$ and the minimum was 5.05 $N \cdot A^{-1}$.

3) Piston Compliance: The compliance of the piston was measured using an electromechanical test instrument (Instron 5866). Epoxy was drawn into the ampoule up to the 0.05 mL mark and allowed to cure; the cured epoxy prevented the ampoule from compressing under load. Compression length

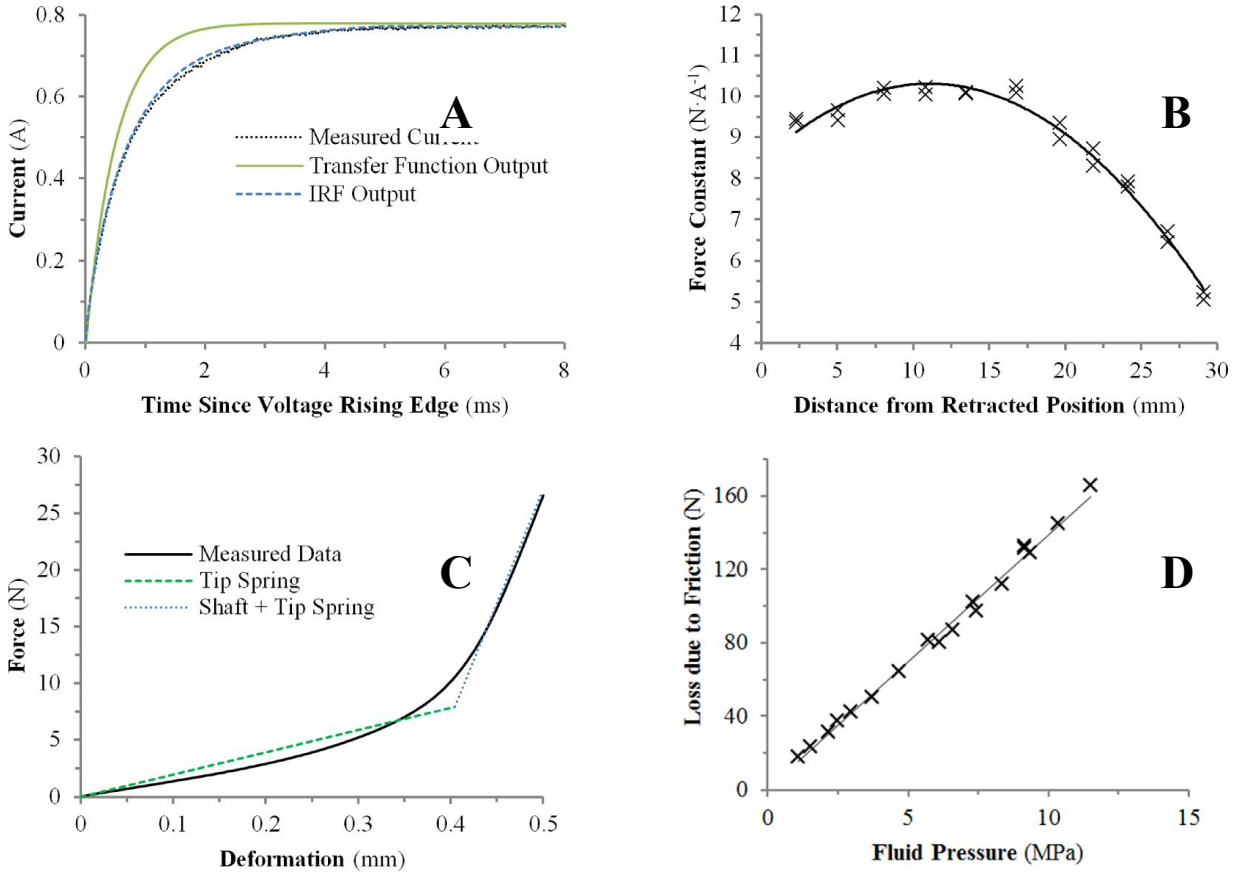

Fig. 3 – A – The current response to a 7.25 V voltage step (black dots), in comparison to the predicted current response to the same voltage step of a 1/(Ls+R) transfer function (green line) and using the impulse response function (blue dotted line). B – The results of force constant tests over the stroke range of the JI (cross) and a fitted 2nd order polynomial with R^2 = 0.9815 (line). C - Fit of piecewise linear piston compliance (tip compliance - green dashed line, shaft compliance - blue dotted line) to measured compression data (black line). D - The fit of the friction coefficient multiplied by the area of tip contact to the loss attributed to friction (cross) across the range of pressures with R^2 = 0.9940.

was monitored and recorded up to a compressive force of 120 N. The non-linearity of piston compliance was modelled with a piecewise linear function that captured both the rubber piston tip compliance and the compliance of the polycarbonate shaft. The piecewise linear function shown in Fig. 3C detemines the value of k_P. When the piston tip is compressing (up to 0.4 mm), a spring constant of 20 kN·m^{-1} is used and, once the tip compressed, a spring constant of 200 kN·m^{-1}, representative of the stiffness of the piston shaft alone, is used. The fit exhibited in Fig. 3C demonstrated RMS error of 0.86 N over the first 0.5 mm of deformation.

4) Friction: Static friction was given by the force required to initiate piston motion. Sliding friction (F_{FR}) was measured by applying a voltage to the motor (with attached water-filled ampoule) for a period of 20 ms, and determining the steady-state force during the last 5 ms of the test. Eighteen tests were undertaken using a piston and ampoule with the applied voltage ranging from 20 V to 250 V. The sliding friction was determined by subtracting from F_{FR} the force required to eject water through the orifice (given by the solution of Equation 4). This method assumes that water is inviscid and that all losses when ejecting water can be attributed to sliding friction. The area of contact (A_C) between the piston tip and ampoule was measured during the compression test at a force of 170 N, a value similar to the force applied to the piston during an injection. The fit of the friction model (3) to the measurements of force less the Bernoulli loss (Fig. 3D) exhibited an RMS error of 3.35 N. This value is 4 % of the average friction value. The static friction was a small percentage of the total friction (Table I).

5) Ampoule and Fluid Compliance: The effective bulk modulus of the ampoule and its contained fluid was determined by applying a force of 200 N to the fluid, corresponding to a fluid pressure of 20 MPa. The piston compression was subtracted from the coil displacement, and the remaining displacement attributed to ampoule and fluid compliance. This displacement was converted into an increase in volume of the ampoule. The pulse tests were repeated over a range of starting positions from 25 mm to 10 mm from the end of the ampoule. The equation

$$K_{AF} = V_F \frac{dP_F}{dV_F}, \tag{7}$$

where V_F *i*s the volume of fluid in the ampoule, allowed the effective ampoule and fluid bulk modulus to be calculated after each test. The average value of the combined fluid and ampoule bulk modulus was calculated to be 649 MPa with a standard deviation of 12.8 MPa across six tests.

6) Pressure Loss across Orifice: Solutions of glycerol (30 %, 60 %, 75 %, and 85 % glycerol by volume) and water were used to form a series of fluids of different viscosities, and were subjected to pulse tests of 20 ms duration ranging between 60 V and 260 V. The viscosity of each glycerol-water solution was evaluated using a rheometer (TA Instruments AR1000) at the MIT Hatsopolous Microfluids Laboratory. The viscosity of the solutions was 0.0022 Pa·s (30 % glycerol), 0.0125 Pa·s (60 % glycerol), 0.0423 Pa·s (75 % glycerol), and 0.1090 Pa·s (85 % glycerol). The pressure on the fluid was determined by subtracting the friction force from the coil force (estimated from the current and the force constant of the motor at the average position over the last 5 ms of the test (see Fig. 3B)), and dividing by the area of the piston. The steady state coil speed was calculated from the last 5 ms of position data; this speed was converted into an average jet speed using the area ratio between the piston and the orifice. The difference between the pressure actually developed during the test and the value calculated from the jet speed using the Bernoulli equation is the pressure drop over the orifice structure. Equation (5) was used to evaluate the K_D value for the test. The value determined for the discharge coefficient ranged from 0 (for water) to 0.35 (for 85 % glycerol). The nature of the relationship between viscosity and discharge coefficient has been represented by a variety of power, logarithmic and polynomial laws operating on the Reynolds number of the fluid [18]–[20]. For our data, shown in Fig. 5, the relationship is represented by a log-linear model with viscosity normalized to water as the dependent variable (n = 8). The equation of the model fit is

$$K_D = 7.27 \times 10^{-2} \ln\left(\frac{\mu}{\mu_W}\right) + 3.88 \times 10^{-3}, \tag{8}$$

where μ is the viscosity of the fluid and μ_W is the viscosity of water (0.001 Pa·s). The standard error of the log coefficient is 1.49×10^{-3} and the standard error of the constant is 1.06×10^{-2}.

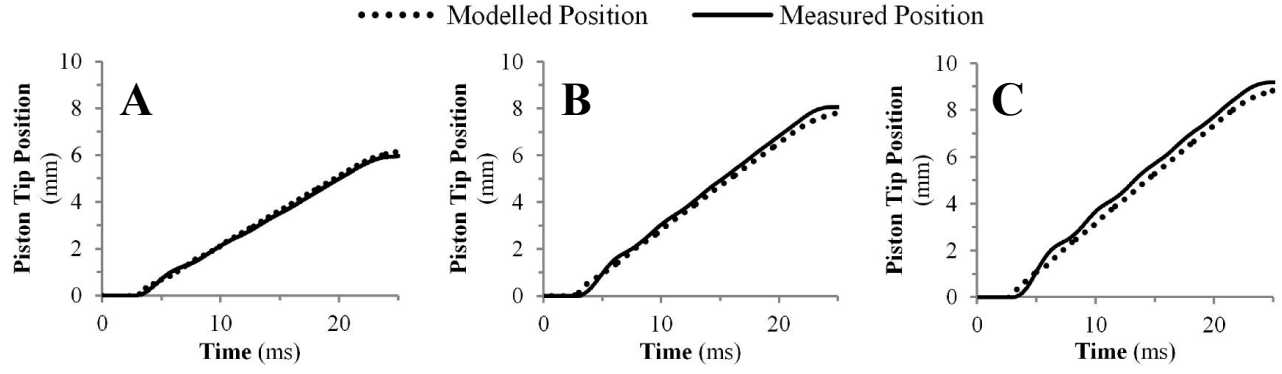

Fig. 4 - The results of three piston-tracking experiments conducted during pulse tests of 120V (A), 200V (B) and 260V (C). The dotted line is the model prediction and the solid line represents the measured position from the tracking software. The fluid used was water.

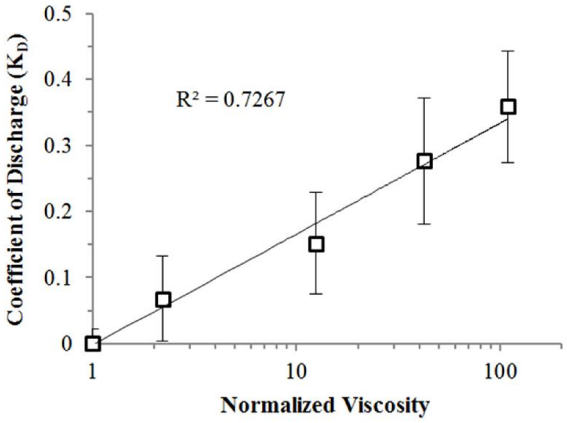

Fig. 5 - Plot of discharge coefficient (K_D) over the range of viscosities tested. A model fit is represented by the black line with $R^2 = 0.727$.

TABLE I
EMPIRICAL PARAMETER VALUES

NAME OF PARAMETER	Value
Coil Mass	0.050 kg
Piston Diameter	3.57 mm
Piston Spring Constant	201 kN·m^{-1}
Maximum Rubber Tip Deformation	0.400 mm
Effective Tip Spring Constant	20.0 kN·m^{-1}
Area of Tip Contact	5.60E-5 m^2
Combined Bulk Modulus	6.49E+8 Pa
Fluid Density	1000 kg·m^{-3} – 1260 kg·m^{-3}
Sliding Friction Coefficient	0.240
Static Friction	1.50 N
Viscosity	0.001 Pa·s – 0.100 Pa·s
Discharge Coefficient	0.000 – 0.350

III. VALIDATION

The model uses knowledge about the elements of the system to predict the piston tip displacement profile over time. Direct measurements of piston tip position can thus verify that the model is correctly incorporating the effects of system parameters. The model also predicts the jet speed as a function of time, which can be compared to estimates of jet speed inferred from the force of the jet as it impacts on a load cell.

1) Piston Tip Measurements: A Phantom v9 CMOS high-speed camera was used to measure the piston tip position during pulse tests of voltage amplitude between 120 V and 250 V, and 20 ms duration. The voltage was pre-filtered using a 2nd Order Butterworth low-pass filter with a cut-off frequency of 125 Hz. Video was captured at 10,000 fps and the tip was followed in one dimension using the program Tracker (Douglas Brown, Cabrillo College). The results shown in Fig. 4 exhibit RMS error of 0.09 mm, 0.23 mm and 0.38 mm for 120 V, 200 V and 250 V pulse tests respectively. The error was calculated over 25 ms from the initiation time of the pulse test to include the relaxation of compliant elements.

2) Jet Force Measurement: A 225 V filtered pulse was applied for 20 ms while a contact force sensor (FUTEK LSB200, resonant frequency of 3000 Hz) was placed perpendicular to the jet, 1.4 mm from the orifice. The decrease in speed (and pressure) as the jet traveled the standoff distance was expected to be minimal. The jet force was measured with a 20 kHz sample rate, converted into a pressure P by assuming the jet had the same area as the orifice, and then into a measurement of jet speed using

$$u_O = \sqrt{\frac{2P}{\rho}}. \quad (9)$$

The measured jet speed matches the model prediction with an RMS error of 18.0 m·s^{-1} over the 30 ms following pulse initiation (Fig. 6). Most of the error is due to the difference in the amplitude of oscillations between the results. The modeled jet speed overshoots by 44 %, whereas the estimated actual jet speed overshoots by only 26 %. The frequency of these oscillations has been correctly predicted although the level of damping is greater in the measured jet speed profile.

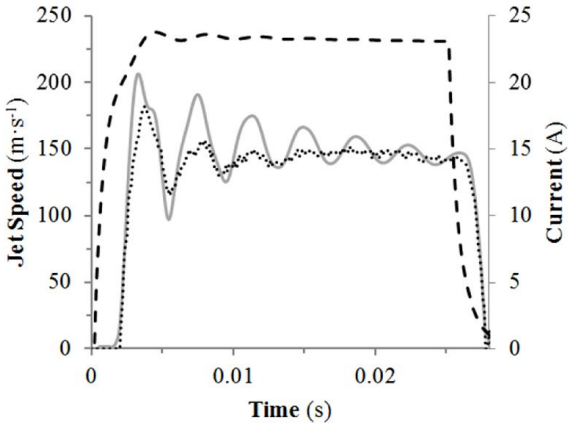

Fig. 6 - Comparison of measured jet speed calculated from jet impact upon force plate (dotted black line) and model predictions (grey line). The current is presented as a dashed black line.

IV. DESIGN PREDICTIONS

The model can be used to predict the effect of changing parameters that characterize the behavior of the device. The model was run with a range of piston spring constants, friction coefficients, ampoule bulk moduli, and viscosities to establish the behavior changes that are attributable to these particular parameters. For each run, the input was a 20 ms pulse of 200 V, with all parameters other than the one being tested set according to Table I. The default fluid was water, for which the viscosity was set to 0.001 Pa·s, the discharge coefficient was set to 0 and the fluid density was 1000 kg·m^{-3}.

Fig. 7 indicates how changing parameters affect the behavior of the device. Increasing the piston spring constant has little effect on the jet speed (Fig. 7A), but the coil rise time and oscillation period both decrease. Increasing coil friction (Fig. 7B) reduces the steady state and maximum jet speeds and slightly decreases the rise-time, but not the period, of coil position oscillations. When the bulk modulus of the ampoule is increased (Fig. 7C), decreased oscillatory behavior is evident in the jet speed and the coil position, corresponding to a reduction in overshoot. The period of coil position oscillation and the rise time decreases with increasing bulk

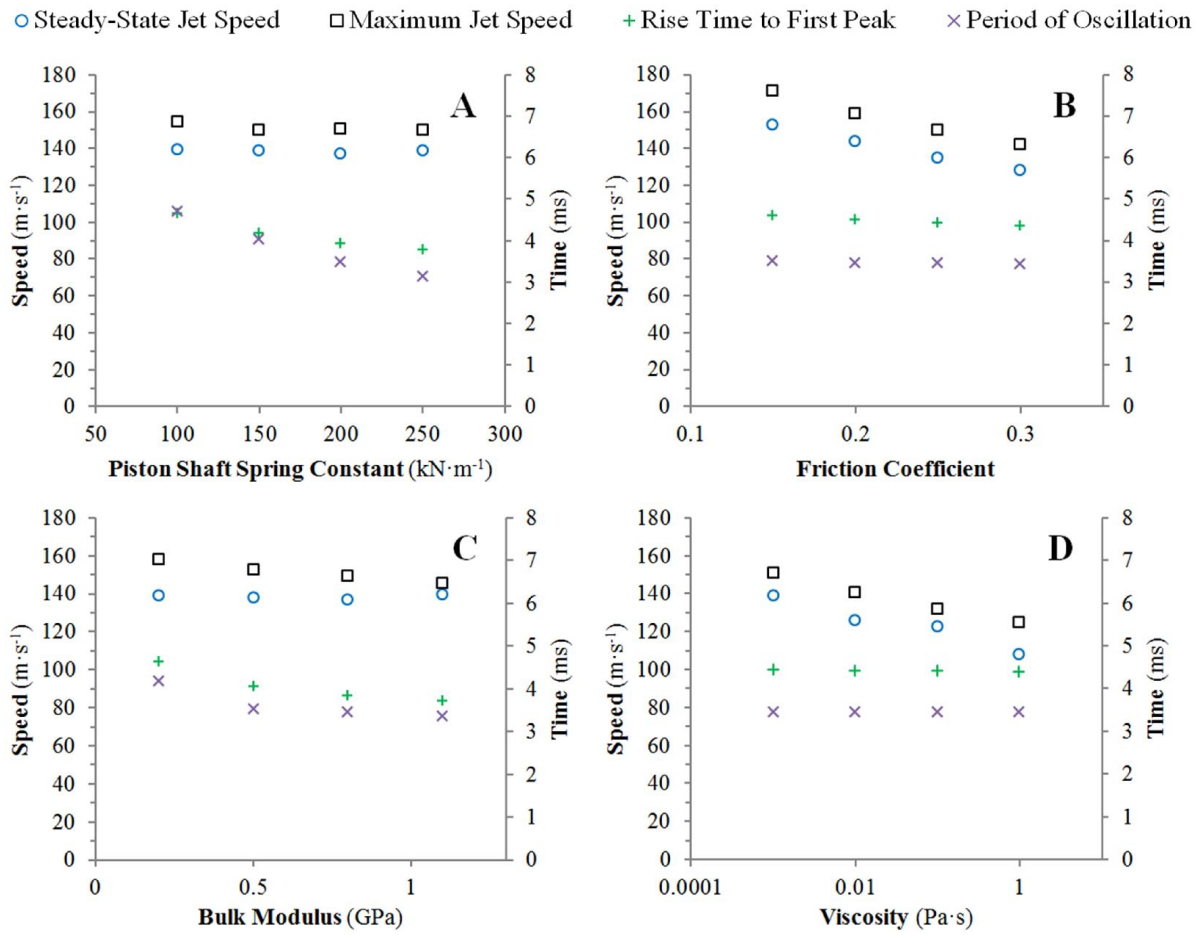

Fig. 7 - Steady state jet speed (blue circles), maximum jet speed (black squares), rise time to first peak of position profile (green plus signs), period of coil position oscillations (purple crosses) when model parameters are modified. These parameters are piston spring constant (A), friction coefficient (B), ampoule bulk modulus (C), and viscosity (D).

modulus. As viscosity increases (Fig. 7D), the steady state jet speed and maximum jet speed both decrease and the overshoot slightly increases. The decrease in coil rise time evident when friction was increased is not seen when viscosity is increased.

V. Discussion

The use of stochastic techniques to estimate the impulse response function allowed for the rise time of the modeled current to match measured current. As a result, the frequency of oscillations in modelled coil and piston tip position was well-aligned, providing a more accurate prediction of JI behavior.

Sliding friction in the injector system occurs between the rubber piston tip and the inside surface of the polycarbonate ampoule. A review of the literature indicates that we should expect the friction coefficient between these surfaces to be between 0.2 and 0.3 [21]–[23]. The friction model presented fits well (Fig. 3D) and the estimated friction coefficient is within the expected range (Table I) when all losses with water are attributed to friction. We conclude that this attribution is valid in the context of the model.

The discharge coefficient results show a reasonable level of standard error for the fit coefficients. The error is indicative of the nature of the fluids as variable in the magnitude of their internal impedance. It is clear that the effect of increased viscosity is significant; in the pulse tests, jet speed reduces from 143 ms^{-1} to 109 ms^{-1} as viscosity is increased from 0.001 Pa·s to 0.1 Pa·s (Fig. 7D). Previous published tests by other authors [24] indicate that this reduction in jet speed would lead to greatly reduced probability of successful delivery. It is likely that more power or modifications to the current device will be required to effectively deliver fluids of 0.1 Pa·s viscosity and above The current portable device is capable of jet injections of fluids of up to 0.1 Pa·s viscosity, though it is restricted by the size of the attached amplifiers. We are pursuing the development of portable amplifiers as well as portable jet injectors that exhibit a higher force constant to extend the ability of the device to new applications.

Piston tip measurements can better predict the jet speed profile as the effect of piston compliance is removed (Fig. 4). The model predicts much smoother profiles than the measured profiles but the discrepancy can be attributed to the noise present in the high-speed camera images. The results indicate that the oscillations evident in coil position are not coupled

through to the piston tip position. We conclude that when a compliant piston is used, the coil position cannot be relied upon to provide an acceptable estimate of jet speed during the dynamic phase of jet injection.

The jet force measurements (Fig. 6) show a reasonable fit between the force plate measurement and model predictions. The oscillation amplitude and the damping of the oscillations is less accurately predicted than the steady-state jet speed and the rise to that jet speed, likely due to the variability in the response of the compliant elements in the system. Alternatively, the force transducer used may not have had the necessary frequency response required to pick up the magnitude of the oscillations in the jet speed.

The model can be used to inform design decisions for future development of jet injectors. As the device used in the experiments is primarily used for fluids with viscosities near to that of water, the model can be used to identify areas of improvement for future viscous-drug devices. The effect of piston compliance on the developed jet speed is negligible; this is despite significant variation in the amplitude of fluctuations for the coil position. Hence, a stiffer piston allows the potentiometer to better estimate the fluid volume and jet velocity, and tighter coupling between coil speed and jet speed.

Variation of the input parameters revealed the dominant second-order nature of the system. An important parameter to reduce when trying to control the jet speed is the overshoot, and it is clear that the compliance of the ampoule plays a major role in its determination. A stiffer ampoule will produce a steady-state jet speed much earlier than with the original compliant set-up. It is easier to achieve control of injection depth when the jet speed is tightly controlled, as a relationship between jet speed and injection depth can be identified [8], [25]. Therefore, a stiffer ampoule will help with producing a smoother, more effective jet for delivery.

If the sliding friction coefficient is reduced, the jet speed increases with no change in the input energy from the coil. We anticipate that much would be gained from pursuing an investigation into how to reduce the sliding friction coefficient. Achieving this would increase the efficiency of the system, allowing higher speed jets to be formed more easily, regardless of viscosity.

The modeling will guide the future development and use of the device. The first improvement that we pursue will be stiffening the ampoule and piston to improve the control and shape of the jet speed profile over time. Secondly, we will take advantage of the controllability of our system to rate-limit the application of force to the coil and thus avoid exciting excessive jet-speed overshoot. After this, an investigation of the effect of orifice diameter and the geometry of the ampoule on the discharge coefficient will guide us in choosing the best shape through which to force the fluid.

VI. Conclusions

The jet injector electromechanical model presented in this article expands upon previous knowledge by better characterizing the electrical system, expanding the modeling of compliance to include the ampoule, and taking account of the loss due to the viscosity of the injected fluid. Throughout the characterization of the JI presented in this paper, we focused on identifying the elements of the system that most affect its performance when jet-injecting viscous fluids. We identified these as the friction coefficient, the compliance of the JI components, and the properties of the fluid being injected. The model provides a better prediction of the jet speed profile over time than that provided by a direct conversion of coil speed to jet speed. The insight that the model provides into jet development will be used to develop methods that improve the reliability of jet injection, focusing on delivering fluid to a particular layer underneath the skin surface with a targeted jet.

References

[1] M. A. F. Kendall, “Drug Delivery,” *Handb. Exp. Pharmacol.*, vol. 197, pp. 193–219, 2010.

[2] S. Mitragotri, “Current status and future prospects of needle-free liquid jet injectors,” *Nat. Rev. Drug Discov.*, vol. 5, no. 7, pp. 543–548, 2006.

[3] A. Gursoy et al., “Needle-free delivery of lidocaine for reducing the pain associated with the fine-needle aspiration biopsy of thyroid nodules: time-saving and efficacious procedure.,” *Thyroid*, vol. 17, no. 4, pp. 317–321, Apr. 2007.

[4] U. Schneider et al., “Painfulness of needle and jet injection in children with diabetes mellitus,” *Eur. J. Pediatr.*, vol. 153, no. 6, pp. 409–410, 1994.

[5] E. L. Giudice and J. D. Campbell, “Needle-free vaccine delivery.,” *Adv. Drug Deliv. Rev.*, vol. 58, no. 1, pp. 68–89, Apr. 2006.

[6] W. Walther et al., “Uptake , Biodistribution , and Time Course of Naked Plasmid DNA Trafficking After Intratumoral In Vivo Jet Injection,” *Hum. Gene Ther.*, vol. 17, no. June, pp. 611–624, 2006.

[7] J. R. Schramm-Baxter and S. Mitragotri, “Investigations of needle-free jet injections.,” in *Proceedings of the Annual International Conference of the IEEE Engineering in Medicine and Biology Society*, 2004, vol. 5, pp. 3543–6.

[8] J. Baxter and S. Mitragotri, “Jet-induced skin puncture and its impact on needle-free jet injections: experimental studies and a predictive model,” *J. Control. Release*, vol. 106, no. 3, pp. 361–373, 2005.

[9] J. C. Stachowiak et al., “Piezoelectric control of needle-free transdermal drug delivery,” *J. Control. Release*, vol. 124, no. 1–2, pp. 88–97, 2007.

[10] A. Taberner et al., “Needle-free jet injection using real-time controlled linear Lorentz-force actuators,” *Med. Eng. Phys.*, vol. 34, no. 9, pp. 1228–1235, Jan. 2012.

[11] O. Stumpp and A. Welch, “Injection of glycerol into porcine skin for optical skin clearing with needle-free injection gun and determination of agent distribution using OCT and fluorescence microscopy,” *Proc. SPIE*, vol. 4949, pp. 44–50, 2003.

[12] J. Liu et al., “Reversible self-association increases the viscosity of a concentrated monoclonal antibody in aqueous solution,” *J. Pharm. Sci.*, vol. 94, no. 9, pp. 1928–1940, Sep. 2005.

[13] M. X. Yang et al., “Crystalline monoclonal antibodies for subcutaneous delivery.,” *Proc. Natl. Acad. Sci. U. S. A.*, vol. 100, no. 12, pp. 6934–9, Jun. 2003.

[14] A. B. Baker and J. E. Sanders, “Fluid mechanics analysis of a spring-loaded jet injector.,” *IEEE Trans. Biomed. Eng.*, vol. 46, no. 2, pp. 235–42, Feb. 1999.

[15] R. M. J. Williams et al., “A computational model of a controllable needle-free jet injector,” *Proc. Annu. Int. Conf. IEEE Eng. Med. Biol. Soc. EMBS*, vol. 2012, pp. 2052–2055, Jan. 2012.

[16] K. Chen et al., “Stagnation Pressure in Liquid Needle-Free Injection: Modeling and Experimental Validation,” *Drug Deliv. Lett.*, vol. 1, no. 1, pp. 97–104, 2011.

[17] F. F. Abdelall et al., “Pressure drop caused by abrupt flow area changes in small channels,” *Exp. Therm. Fluid Sci.*, vol. 29, no. 4, pp. 425–434, Apr. 2005.

[18] F. Numachi et al., “Cavitation effect on the discharge coefficient of the sharp-edged orifice plate,” *J. Basic Eng.*, vol. 82, no. 1, pp. 1–6, 1960.

[19] F. C. Johansen, “Flow through Pipe Orifices at Low Reynolds Numbers,” *Proc. R. Soc. A Math. Phys. Eng. Sci.*, vol. 126, no. 801, pp. 231–245, Jan. 1930.

[20] A. Lichtarowicz et al., “Discharge coefficients for incompressible non-cavitating flow through long orifices,” *J. Mech. Eng. Sci.*, vol. 7, no. 2, pp. 210–219, 1965.

[21] B. N. J. Persson, *Sliding Friction: Physical Principles and Applications*, 2nd ed. Berlin, Germany: Springer-Verlag, 2001.

[22] D. S. Pinchuk, “Friction coefficient of rubber with respect to some types of plastics,” *Chem. Pet. Eng.*, vol. 6, no. 5, pp. 416–417, 1970.

[23] D. I. James, “Rubbers and plastics in shoes and flooring: the importance of kinetic friction,” *Ergonomics*, vol. 26, no. 1, pp. 83–99, 1983.

[24] J. Schramm and S. Mitragotri, “Transdermal drug delivery by jet injectors: energetics of jet formation and penetration,” *Pharm. Res.*, vol. 19, no. 11, pp. 1673–1679, 2002.

[25] J. C. Stachowiak et al., “Dynamic control of needle-free jet injection,” *J. Control. Release*, vol. 135, no. 2, pp. 104–112, 2009.